Scaling relation between renormalized discharge rate and capacity in Na x CoO2 films

Ayumu Yanagita, Takayuki Shibata, Wataru Kobayashi, and Yutaka Moritomo

Citation: APL Mater. **3**, 106104 (2015); doi: 10.1063/1.4933236
View online: http://dx.doi.org/10.1063/1.4933236
View Table of Contents: http://scitation.aip.org/content/aip/journal/aplmater/3/10?ver=pdfcov
Published by the AIP Publishing

Scaling relation between renormalized discharge rate and capacity in Na_xCoO_2 films

Ayumu Yanagita,[1] Takayuki Shibata,[1,2] Wataru Kobayashi,[1,2] and Yutaka Moritomo[1,2,3,a]

[1]*Graduate School of Pure and Applied Science, University of Tsukuba, Tsukuba 305-8571, Japan*
[2]*Institute of Pure and Applied Science, University of Tsukuba, Tsukuba 305-8577, Japan*
[3]*Center for Integrated Research in Fundamental Science and Engineering (CiRfSE), University of Tsukuba, Tsukuba 305-8571, Japan*

(Received 9 September 2015; accepted 4 October 2015; published online 19 October 2015)

Layered cobalt oxide, P2-Na_xCoO_2, is a prototypical cathode material for sodium-ion secondary battery. We systematically investigated the rate dependence of the discharge capacity (Q) in three thin films of $Na_{0.68}CoO_2$ with different film thickness (d) and in-plane grain radius (r). With subtracting conventional voltage drop effect on Q, we derived an intrinsic rate dependence of Q. We found a scaling relation between the renormalized discharge rate ($\gamma \equiv r^2/DT$; D and T are the Na^+ diffusion constant and discharge time, respectively) and relative capacity ($=Q/Q_0$; Q_0 is the value at a low rate limit). The observed scaling relation is interpreted in terms of the Na^+ intercalation process at the electrolyte-Na_xCoO_2 interface and Na^+ diffusion process within Na_xCoO_2. [http://dx.doi.org/10.1063/1.4933236]

Sodium-ion secondary battery (SIB) is a promising candidate for the next-generation battery with environmentally friendly and low-cost characteristics,[1] because it stores the electric energy utilizing the intercalation/deintercalation process of abundant Na^+ (Clarke number[2] = 2.63), instead of the rare Li^+ (0.006). In this sense, the SIB is suitable for large-scale battery for stable use of the solar and/or wind power energies. Komaba *et al.*[3] reported that hard carbon is a promising anode material for SIB, because it shows a high capacity (≥200 mAh/g) and a good cyclability. This finding opens the door to the commercial utilization of SIBs and stimulates the investigation and exploration of cathode materials for SIBs. Among the cathode materials for SIBs, the layered transition metal oxides (Na_xMO_2, where M is transition metal), e.g., P2-type $Na_x[Fe_{1/2}Mn_{1/2}]O_2$[4] and $Na[Fe_{1/2}Co_{1/2}]O_2$[5] with α-$NaFeO_2$ structure, show promising cathode properties.

Among Na_xMO_2, the most intensive investigation has been performed on Na_xCoO_2 with P2-type structure ($P6_3/mmc$, $Z = 2$). This is because it shows interesting structural,[6–10] thermoelectric,[11] and superconductive[12] properties as well as the cathode properties[13] for SIBs. Especially, $Na_{0.7}CoO_2$ shows promising electrochemical properties: a discharge capacity of 130 mAh/g and an average operating voltage of ~2.5 V against Na. In the P2-type structure, the edge-sharing MO_2 layer and Na sheet are alternately stacked. The close-packed oxygen sheets stack as AB|BA, in sharp contrast to the AB|CA|BC stacking in the α-$NaFeO_2$ structure. As a result, the Na site is surrounded by the oxygen triangular prism. Shibata *et al.*[14] fabricated thin films of P2-Na_xCoO_2 on a Au collecting electrode by the pulsed laser deposition (PLD) method. They determined the Na^+ diffusion constant (D) of P2-Na_xCoO_2 by means of the electrochemical impedance spectroscopy (EIS).[15,16] Importantly, the rate property of P2-Na_xCoO_2 becomes excellent in the film form: the discharge capacity (Q) is discernible even at 400 C[14] in film while it disappears above ~10 C in conventional powder. The excellent rate property is ascribed to the good electric contact between

[a]Author to whom correspondence should be addressed. Electronic mail: moritomo.yutaka.gf@u.tsukuba.ac.jp

the collector electrode and respective Na_xCoO_2 grains. In this sense, the film electrode gives us an ideal platform to investigate the effect of the Na^+ transfer and diffusion processes on Q. In our previous paper,[17] we have investigated the discharge curves in thin films of three layered oxides, i.e., P2-$NaCoO_2$, P2-$NaMnO_2$, and O3-$NaCoO_2$. By assuming one dimensional (1D) Na^+ diffusion along the film thickness, we analyze the interrelation between the renormalized discharge rate ($\gamma \equiv d^2/DT$; d is the film thickness) and relative capacity ($=Q/Q_0$).

In order to determine the length scale which governs the Na^+ diffusion processes and Q, we systematically investigated the rate dependence of the discharge curves in thin films of P2-$Na_{0.68}CoO_2$ with different deposition time. By subtracting conventional voltage drop effect on Q, we derived an intrinsic rate dependence of Q. We found that Q/Q_0 scales well with r^2/DT (r is the in-plane grain radius), not d^2/DT. This indicates that Q is governed by the intra-grain Na^+ diffusion, not by the 1D Na^+ diffusion along the film thickness. We demonstrate that the two dimensional (2D) diffusion equation quantitatively reproduces the scaling relation, including the characteristic γ ($\gamma_c \sim 3$), where Q/Q_0 becomes 1/2.

Thin film of P2-$Na_{0.68}CoO_2$ was grown on Au-deposited MgO (100) substrate at 923 K in an oxygen partial pressure of 50 Pa for 10, 30, and 60 min. by the PLD method. The targets were prepared by solid state reaction. First, Na_2CO_3 and Co_3O_4 were mixed in 0.7:1.0 atomic ratio and calcined at 1073 K for 12 h in air. Then, the powder was finely ground, pressed into pellet of 2 mm in diameter, and calcined at 1073 K for 12 h in air. The second harmonics of an yttrium-aluminum-garnet (YAG) pulse laser was used as excitation light source. The pulse energy, repetition frequency, and wavelength were 1.7 J/cm^2, 10 Hz, and 532 nm, respectively. The distance between the target and the substrate was 35 mm. The film thicknesses (d) were, 80, 274, and 575 nm, which were determined by cross-sectional SEM image or by a contact profilometer. The film area was 0.5 cm^2. The as-grown P2-$Na_{0.68}CoO_2$ film is stable in air. Figure 1 shows the X-ray diffraction patterns of the films. All the reflections can be indexed by the P2-type structure ($P6_3/mmc$, $Z = 2$). The intense (002) and (004) reflections indicate the (001)-orientation of the films. The mass of the active material was estimated by d and the actual density (=2.3 g/cm^2) of the film. The sodium concentration ($x = 0.68$) of the target was determined by Rietveld analysis[18] of the X-ray powder diffraction pattern, which was obtained at BL02B2 beamline at SPring-8.[19] x(=0.68) of the film was assumed to be the same as the target.

The discharge properties of the films were investigated using a two-pole beaker type cell with a battery charge/discharge system (HOKUTO HJ-SD8). The cell was made by a glass vessel with screw cap, on which two copper wires were stuck and sealed with Araldite. The film (cathode) and Na (anode) were attached at the inner edges of the wires. The electrolyte was 1M $NaClO_4$ in propylene carbonate (PC). The lower and upper cut-off voltages vs. Na were 2.0 V and 3.4 V, respectively. The charge current was fixed at 1 μA/cm^2, which corresponds to 0.5, 0.14, and 0.06 C at d = 80, 274, and 575 nm, respectively. All the experimental procedures were performed in a glove box.

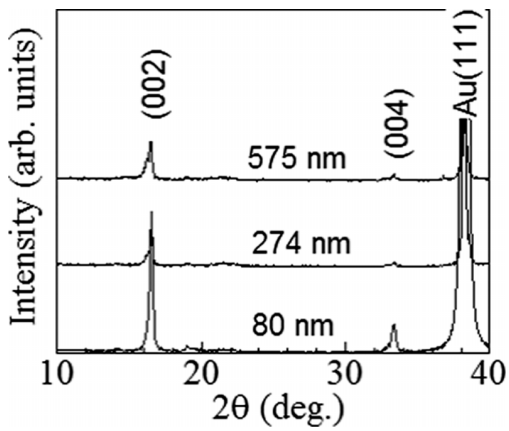

FIG. 1. X-ray diffraction patterns of thin films of P2-$Na_{0.68}CoO_2$ with different thickness (d). X-ray source was the Cu Kα line. Values in parentheses represent indexes in the $P6_3/mmc$ setting.

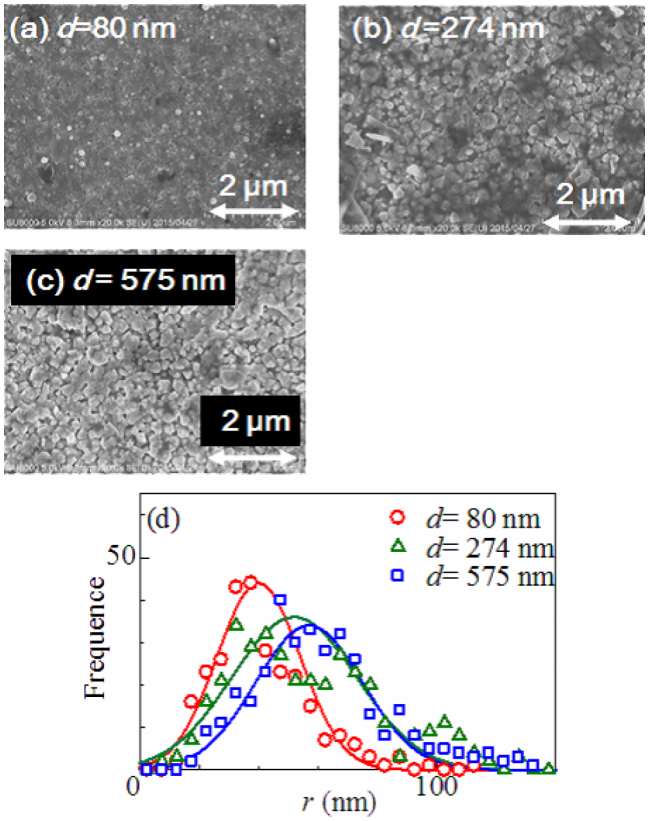

FIG. 2. SEM images of thin films of P2-$Na_{0.68}CoO_2$ with different thickness (d): (a) d = 80 nm, (b) 274 nm, and (c) 575 nm. (d) Histograms of the grain radius (r). Curves represent least-squares fittings with a Gauss function.

Figures 2(a)–2(c) show SEM images of the $Na_{0.68}CoO_2$ films with different thickness (d). The SEM images were obtained with SU8020 at Faculty of Pure and Applied Science and the OPEN FACILITY, Research Facility Center for Science and Technology, University of Tsukuba. Figure 2(d) shows the histograms of the in-plane grain radius (r). The 80 nm film consists of smaller grains ($r = 40 \pm 14$ nm), as shown by a solid curve in Fig. 2(d). On the other hand, the 274 and 575 nm films consist of larger grains ($r = 52 \pm 21$ and 57 ± 18 nm) reflecting the longer deposition time. One may doubt that the grain size changes after the deintercalation/intercalation process via the volumetric expansions and/or amorphization processes. We note that the grain size shows negligible change even after 1000 charge/discharge processes.[14]

Figure 3(a) shows discharge curve of the 80 nm film. The discharge curve at a low rate limit (=1.5 C) shows abrupt voltage drops at 0 and 40 mAh/g. The abrupt drops are ascribed to the single phase points while the regions sandwiched by the drops are ascribed to the two-phase regions. Actually, the abrupt drops at 0 mAh/g and 40 mAh/g correspond to the $x = 1/2$ and 3/2 order phase, respectively.[9] Similar features are observed in the other films [Figs. 3(b) and 3(c)].

In all the films, the capacity at 2.0 V systematically decreases with increase in the discharge rate. The reduction of the capacity is mainly ascribed to the voltage drop, because the discharge curve shifts to the low voltage side with increase in the rate. The voltage drop is expressed as - IR, where R and I are the battery resistance and current density, respectively. Figure 4 shows the voltage drops ($|\Delta V|$) at 0 mAh/g against I. $|\Delta V|$ well obeys the ohmic law. R is estimated to be 250, 230, and 240 Ω cm^2 at d = 80, 274, and 575 nm, respectively. R is nearly independent of d, suggesting that R is mainly originated in the electrolyte.

Looking carefully at the rate dependence of the discharge curve (Fig. 3), we found that the shape of the discharge curve changes with the discharge rate. For example, in the 80 nm film [Fig. 3(a)], the Q value at 75 C significantly decreases by 30 mAh/g while the position of the abrupt

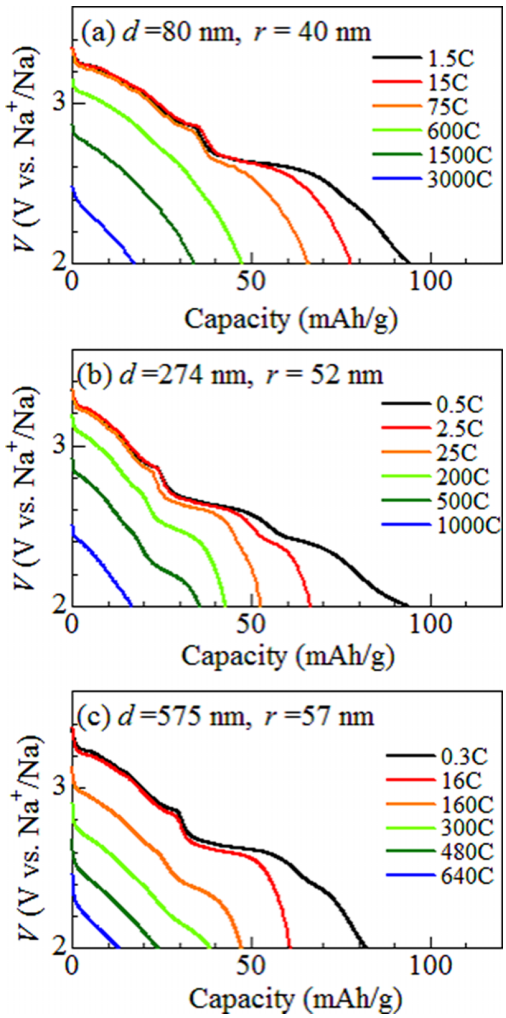

FIG. 3. Discharge curves of thin films of P2-$Na_{0.68}CoO_2$ against thickness (d) and grain radius (r): (a) $d = 80$ nm, (b) 274 nm, and (c) 575 nm.

voltage drop is fixed at 40 mAh/g. Such a deformation of the discharge curve cannot be ascribed to the conventional voltage drop effect. To derive the intrinsic rate dependence of Q, we carefully subtracted the conventional voltage drop effect on Q by changing the lower voltage as $2.5–IR$. Here, note that thus determined Q value would not change if the discharge curve rigidly shifted to the low

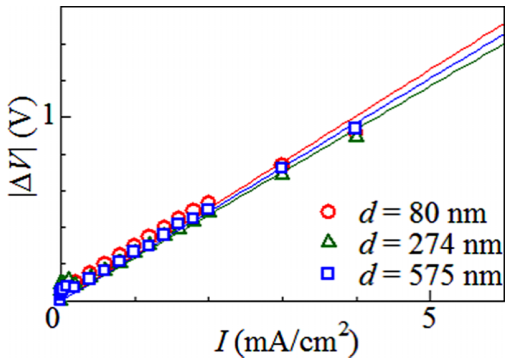

FIG. 4. Voltage drop ($|\Delta V|$) against current density (I) of thin films of P2-$Na_{0.68}CoO_2$. The straight lines are the results of least-squares fittings.

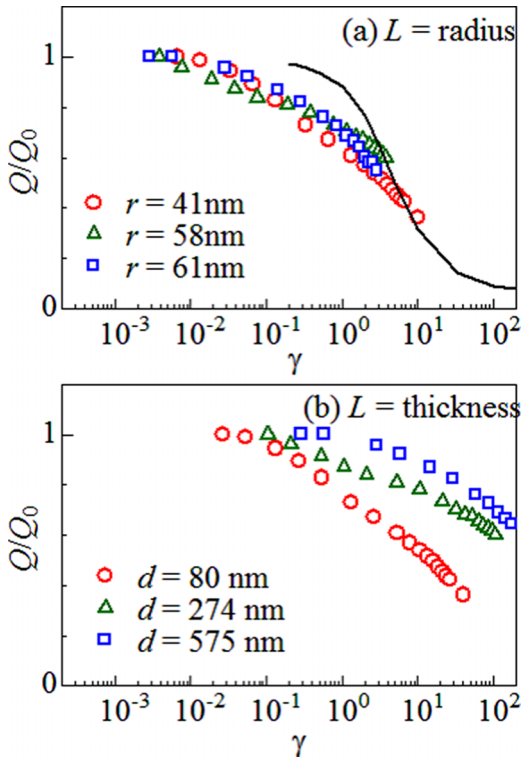

FIG. 5. Relative capacity (Q/Q_0) against renormalized discharge rate (γ): the length scale (L) in γ is (a) in-plane grain radius (r) and (b) film thickness (d). The Q values are evaluated at the lower voltage (=2.5–IR, where I and R are the current density and battery resistance, respectively). The thick solid curves in Fig. 4(a) are derived by the numerical calculation of 2D diffusion equation (see text).

voltage side. We will analyze the rate dependence of Q in terms of Na^+ intercalation and diffusion. Then, it is convenient to change the discharge rate to renormalized one. Let us consider the diffusion equation, $\partial n(t,x)/\partial t = D\partial^2 n(t,x)/\partial x^2$, where $n(t, x)$ is the Na^+ density at t and x. If we introduce dimensionless length and time, i.e., α ($\equiv x/L$; L is the length scale) and β ($\equiv t/T$; T is the time needed for the full discharge), we obtained $\partial n(\beta,\alpha)/\partial\beta = (L^2/DT)^{-1}\partial^2 n(\beta,\alpha)/\partial\alpha^2$. This equation indicates that the diffusion dynamics scales with the renormalized discharge rate ($\gamma \equiv L^2/DT$) irrespective of the individual L, D, and T values. D is a characteristic diffusion constant for the entire discharge process and is set at 1×10^{-12} cm^2/s.

Figure 5 shows the relative capacity (Q/Q_0) against γ ($\equiv L^2/DT$). In Fig. 5(a), we chose the in-plane grain radius (r) as the length scale (L) of γ. We found that the γ-Q/Q_0 plots of the three films trace a universal curve: Q/Q_0 gradually decreases with γ and becomes 0.5 at $\gamma \sim 3$. We note that P2-Na_xCoO_2 has a layer structure and the Na^+ diffusion is confined between the adjacent CoO_2 layers. Then, it is reasonable that the diffusion dynamics is governed by the in-plane grain radius (r). The scaling relation further indicates that the diffusion process mainly governs Q while the intercalation process has minor effects on Q. Roughly speaking, the Na^+ intercalation effect is included as the charge-transfer resistance (R_{CT}) of Na^+ at the electrolyte-Na_xCoO_2 interface. If the voltage drop ($=-R_{CT}I$) due to the intercalation were higher than ~2.5 V, we should observe no capacity. In Fig. 5(b), we chose the film thickness (d) as the length scale (L). We observed no scaling relation between Q/Q_0 and γ. These observations indicate that Q is governed by the intra-grain Na^+ diffusion, not by the 1D Na^+ diffusion along the film thickness.

Overall behavior of the γ-Q/Q_0 curve [Fig. 5(a)] is interpreted as follows. In the discharge process, Na^+ transfers to Na_xCoO_2 at a constant rate ($\propto \gamma$). In the low-γ region ($\ll 10^{-2}$), the Na^+ at the surface region can diffuse into the inner side of the grain before the next Na^+ transfer. Consequently, Na^+ transfer is possible until Q/Q_0 reaches ≈ 1. In the high-γ region ($\gg 10^{-2}$), however, the Na^+ at the surface region cannot diffuse into the inner side before the following Na^+ transfer. In

other words, parts of the surface Na^+ sites are blocked by the residual Na^+ (*surface blocking* effect). This means that the Na^+ transfer is terminated before Q/Q_0 reaches 1, when all the surface sites are blocked. We note that the Na^+ intercalation process further suppresses Q/Q_0 in the high-γ region, because *surface blocking* effect enhances the voltage drop ($=-R_{CT}I/\delta$, where δ is the fraction of the active surface Na^+ site) at the electrolyte-Na_xCoO_2 interface. Thus, the intercalation process terminated the Na^+ transfer even before all the surface sites are blocked.

To visualize the above-mentioned situation, we numerically simulate the discharge process with the 2D diffusion equation. We neglect the effect of electric field as the driving force of the Na^+ diffusion, because Na_xCoO_2 is metallic. In polar coordination with circular symmetry (partial differentials by θ and z are zero), the 2D equation becomes $\frac{\partial n(\beta,\alpha)}{\partial \beta} = \frac{1}{\gamma}[\frac{\partial^2 n(\beta,\alpha)}{\partial \alpha^2} + \frac{1}{\alpha} \cdot \frac{\partial n(\beta,\alpha)}{\partial \alpha}]$, with use of α, β, and γ. The simulation was performed by differential calculus with the space mesh (N_β) of 30 and time mesh (N_α) of 10 000. At the surface of the active material ($\alpha = 0$), we force a constant Na^+ intercalation ($=N_\beta/N_\alpha$). The Na^+ intercalation stops if the density ($=1 - n$) of the Na^+ vacancy at $\alpha = 0$ becomes smaller than N_β/N_α. The β value at this condition corresponds to Q/Q_0. Figure 6(a) shows an example of the Na^+ density (n) profiles against the dimensionless length (α) at low-γ(=1). In this condition, Na^+ at the surface region can diffuse into the inner side of the grain before the next Na^+ transfer. Consequently, Na^+ intercalation is possible above $\beta = 0.8$. Figure 6(b) shows an example of the n-α profiles at high-γ(= 10). In this condition, Na^+ at the surface region cannot diffuse into the inner side before the following Na^+ transfer. As a result, the Na^+ transfer is terminated at $\beta \approx 0.3$ by the surface blocking effect. In Fig. 5(a), we show the calculated results as solid curve. Q/Q_0 steeply decreases as γ increases at $\gamma \sim 3$, reflecting the surface blocking effect. Thus, the simple diffusion model reproduces the global feature of the empirical relation between γ and Q/Q_0. Here, we emphasize that we have no adjustable parameters in both the experiment and calculation. Nevertheless, the diffusion model quantitatively reproduces the characteristic γ ($\gamma_c \sim 3$), where Q/Q_0 becomes 1/2.

Even though the diffusion model reproduces γ_c, the model fails to reproduce the gradual decrease in Q/Q_0 against γ. This is probably because the model fails to include several effects of the actual active material, such as, successive structural phase transition, x-dependence of the crystal structure, x-dependence of D, and inter-Na^+ interaction. For example, P2-Na_xCoO_2 shows several ordering phases of Na^+ at $x = 1/2$ and 2/3.[9] Such orderings of Na^+ cause considerable re-arrangement of the host framework and have serious effects on Q/Q_0. In addition, Na_xCoO_2 shows anomalous compression along c axis with Na^+ intercalation:[6,20] c decreases from 11.3 Å at $x = 0.55$ to 10.5 Å at $x = 1.00$. The anomalous compression is ascribed to the coulombic interaction between the $[Na]^{x+}$ and $[CoO_2]^{x-}$ layers.[20,21] The compression causes the negative feedback for the Na^+ intercalation, and has serious effect on Q. Finally, let us consider how the Na^+ intercalation process

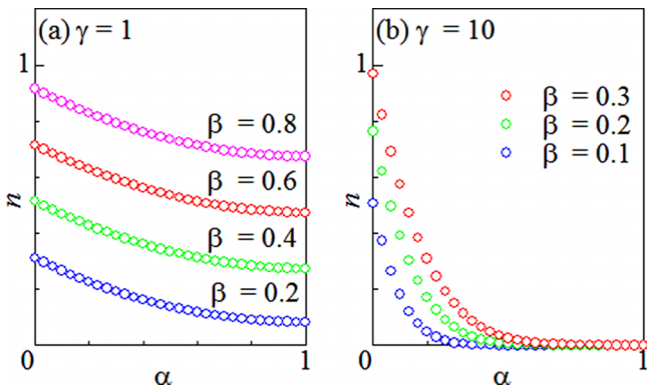

FIG. 6. Results of numerical calculation of 2D diffusion equation, $\partial n(\beta,\alpha)/\partial\beta = \gamma^{-1}[\partial^2 n(\beta,\alpha)/\partial\alpha^2 + 1/\alpha \cdot \partial n(\beta,\alpha)/\partial\alpha]$, against α: (a) $\gamma = 1$ and (b) $\gamma = 10$. $\alpha = 0$ correspond to the circle of the disk, while $\alpha = 1$ does center. The system is fully discharged at $\beta = 1$. The discharge process was simulated by differential calculus with the space mesh (N_α) of 30 and time mesh (N_β) of 10 000. At the surface of the active material ($\alpha = 0$), we force a constant Na^+ intercalation ($=N_\alpha/N_\beta$).

modifies the γ-Q/Q_0 curve. The intercalation process suppresses Q/Q_0 more seriously at higher-γ, since the voltage drop is in proportion to I ($\propto\gamma$) and $1/\delta$. Then, the Q/Q_0-γ becomes steeper if we include the intercalation process.

In summary, we systematically investigated the rate dependence of Q/Q_0 in three films of P2-$Na_{0.68}CoO_2$. By subtracting the conventional voltage drop effect on Q, we found a scaling relation between γ ($\equiv r^2/DT$) and Q/Q_0. We found that the 2D diffusion model quantitatively reproduces the characteristic γ ($\gamma_c \sim 3$), where Q/Q_0 becomes 1/2. Our analysis indicates that diffusion model is a good starting to understand the rate dependence of Q.

This work was supported by a Grant-in-Aid (No. 23684022) for Scientific Research from the Ministry of Education, Culture, Sports, Science and Technology, Japan. The SEM images were obtained with SU8020 at Faculty of Pure and Applied Science and the OPEN FACILITY, Research Facility Center for Science and Technology, University of Tsukuba. The synchrotron-radiation X-ray powder diffraction experiments were performed at the SPring-8 BL02B2 beamline with the approval (No. 2014A1056) of the Japan Synchrotron Radiation Research Institute (JASRI).

[1] S.-W. Kim, D.-H. Seo, X. Ma, G. Ceder, and K. Kang, Adv. Energy Mater. **22**, 710 (2012).
[2] E. W. Clarke and H. S. Washington, "The composition of the earth's crust," U.S. Government Printing Office (1924).
[3] S. Komaba, W. Murata, T. Ishikawa, N. Yabuuchi, T. Ozeki, T. Nakayama, A. Ogata, K. Gotoh, and K. Fujiwara, Adv. Funct. Mater. **21**, 3859 (2011).
[4] N. Yabuuchi, M. Kajiyama, J. Iwatate, H. Nishikawa, S. Hitomi, R. Okuyama, R. Usui, Y. Yamada, and S. Komaba, Nat. Mater. **11**, 512 (2012).
[5] H. Yoshida, N. Yabuuchi, and S. Komaba, Electrochem. Commun. **34**, 60 (2013).
[6] Q. Huang, M. L. Foo, R. A. Pascal, Jr., J. W. Lynn, B. H. Toby, T. He, H. W. Zandbergen, and R. J. Cava, Phys. Rev. B **70**, 184110 (2004).
[7] Y. S. Meng, Y. Himuma, and G. Ceder, J. Chem. Phys. **128**, 104708 (2008).
[8] M. Medarde, M. Mena, J. L. Gavilano, E. Pomjakushina, J. Sugiyama, K. Kamazawa, V. Yu. Pomjakushin, D. Sheptyakov, B. Batlogg, H. R. Ott, M. Mansson, and F. Juranyi, Phys. Rev. Lett. **110**, 266401 (2013).
[9] R. Berthelot, D. Carlier, and C. Delmas, Nat. Mater. **10**, 74 (2010).
[10] X. Li, X. Ma, D. Su, L. Liu, R. Chisnell, S. P. Ong, H. Chen, A. Toumar, J.-C. Idrobo, Y. Lei, J. Bai, F. Wang, J. W. Lynn, Y. S. Lee, and G. Ceder, Nat. Mater. **13**, 586 (2014).
[11] I. Terasaki, Y. Sasago, and K. Uchinokura, Phys. Rev. B **56**, R12685 (1997).
[12] K. Takada, H. Sakurai, E. Takeyama-Muromachi, F. Izumi, R. A. Dalanian, and T. Sasaki, Nature **422**, 53 (2003).
[13] J. J. Braconnier, C. Delmas, C. Fouassier, and P. Hagenmuller, Mater. Res. Bull. **15**, 1797 (1980).
[14] T. Shibata, W. Kobayashi, and Y. Moritomo, AIP Adv. **3**, 032104 (2012).
[15] T. Shibata, W. Kobayashi, and Y. Moritomo, Appl. Phys. Express **6**, 097101 (2013).
[16] T. Shibata, W. Kobayashi, and Y. Moritomo, Appl. Phys. Express **8**, 029201 (2015).
[17] T. Shibata, Y. Fukuzumi, W. Kobayashi, and Y. Moritomo, Sci. Rep. **5**, 9006 (2015).
[18] F. Izumi and K. Momma, Solid State Phenom. **130**, 15 (2007).
[19] E. Nishibori, M. Takata, K. Kato, M. Sakata, Y. Kubota, S. Aoyagi, Y. Kuroiwa, M. Yamakawa, and N. Ikeda, Nucl. Instrum. Methods Phys. Res., Sect. A **467-468**, 1045 (2001).
[20] T. Shimono, D. Tanabe, W. Kobayashi, and Y. Moritomo, J. Phys. Soc. Jpn. **82**, 083601 (2013).
[21] J. Beltran-Huarac, J. Palomino, O. Resto, J. Wang, W. M. Jadwisienczak, B. R. Weiner, and G. Morell, RSC Adv. **4**, 38103 (2014).